Electronic Supplementary Information for

Symmetry-Reduction Enhancement of Nitrate Removal on Record-Breaking Layered Yttrium Hydroxide Adsorbents

*Xinyue Sheng, Yu Wang and Jun Xu**

[†]Tianjin Key Lab for Rare Earth Materials and Applications, School of Materials Science and Engineering & National Institute for Advanced Materials, Nankai University, Tianjin 300350, P.R. China

*Email: junxu@nankai.edu.cn.

Table of Contents

Section S1 Experimental Details

1.1. Sample Synthesis and Adsorption Measurements

Chemicals. $YCl_3·6H_2O$ (99.99 wt%), NaCl (99.80 wt%), NaOH (98.00 wt%), NaBr (98.00 wt%), Y_2O_3 (99.99 wt%), $NaNO_3·12H_2O$ (99.00 wt%), and HBr (99.00 vol%, AR) were acquired from Aladdin and employed without further purification.

Sample Synthesis. The LYH-Cl/LYH-Br composite material was prepared following a previously established protocol from our research group.[1-3] $Y(OH)_3$ was synthesized via alkaline precipitation of $YCl_3·6H_2O$ precursor, following the stoichiometric reaction: $YCl_3·6H_2O + 3NaOH \rightarrow Y(OH)_3(s) + 3NaCl + 6H_2O(l)$. The precipitate was hydrothermally aged at 80°C for 24 h to enhance crystallinity and phase purity.

Adsorption Measurements. 0.1 g of LYH-Cl powder was suspended in 40 mL of $NaNO_3·12H_2O$ solution (i.e., 2.5 g/L adsorbent). Solution pH was systematically adjusted using 1 M HNO_3 or 1 M NaOH aqueous solutions under continuous stirring at 600 rpm. Post-adsorption separation was achieved through centrifugation (10,000 rpm, 15 min) followed by membrane filtration (0.22 μm pore size). Each adsorption experiment was conducted in triplicate except the pH-dependence measurement. Mean values and corresponding standard deviation are shown in the plots. Nitrate concentration quantification was performed via UV-vis spectrophotometry in accordance with Chinese national standards (GB/T 5750.5-2006), with nitrogen uptake calculated from differential nitrate concentrations before and after treatment. The collected solids underwent rigorous characterization through PXRD, FTIR, SEM, XPS, and solid-state NMR analyses to elucidate adsorption mechanisms. Control experiments measuring nitrate adsorption by potential impurities (Y_2O_3 and $Y(OH)_3$) were conducted to validate the intrinsic adsorption performance of LYH-Cl.

Recyclability Test. Desorption experiments were conducted by treating nitrate-adsorbed LYH-Cl with saturated NaCl(aq) or LYH-Br with saturated NaBr(aq) (600 rpm, 12 h). Post-desorption solids were centrifuged (10,000 rpm, 15 min), washed with deionized water, and dried at 60°C. For re-adsorption experiments, 0.1 g regenerated adsorbent was suspended in 40 mL $NaNO_3 \cdot 12H_2O$ solution (500 mg/L NO_3^-, pH 7).

Adsorption Measurements with Competitive Anions. The influence of coexisting anions (Cl^-, Br^-, SO_4^{2-}, PO_4^{3-}, HCO_3^-) was evaluated by suspending 0.1 g adsorbent in 40 mL solution containing NO_3^- (100 mg/L) and individual co-anion (200 mg/L).

Y Leaching Measurements. Y leaching amounts were quantified by ICP-OES analysis of the supernatant obtained after centrifuging (10,000 rpm, 15 min) the desorption solution of nitrate-saturated adsorbents. The supernatant was filtered (0.22 μm nylon membrane) and directly tested for leaching Y.

1.2. Sample Characterizations

PXRD Measurements.

Powder X-ray diffraction (PXRD) analysis was conducted on a Rigaku Ultima IV diffractometer equipped with the Cu K_α radiation ($\lambda = 0.15406$ nm). Data acquisition parameters included a 2θ scanning range of 5 °–65 °, a step size of 0.01 °, and a scan rate of 10 ° min^{-1}.

SEM and EDS Measurements.

Sample morphology and elemental composition were characterized using a field-emission scanning electron microscope (FE-SEM, Thermo Scientific QuattroS) with energy-dispersive X-ray spectroscopy (EDS). Specimens were prepared by adhering powder samples to conductive carbon tape, followed by sputter-coating with a 5 nm Au/Pd layer (Hitachi MC1000, 20 s coating duration). Imaging was conducted at 5 kV accelerating voltage, 6.1 mm working distance, and 10,000× magnification in secondary electron imaging mode.

Zeta Potential Measurements.

Zeta potential measurements were conducted on a Malvern Zetasizer Nano ZS analyzer (Model ZEN3600) using electrophoretic light scattering, with samples dispersed in 1 mM KCl electrolyte at pH 7.0 ± 0.2 to maintain ionic strength consistency.

XPS Measurements.

X-ray photoelectron spectroscopy (XPS) analysis was performed on an ESCALAB 250Xi spectrometer (Thermo Fisher Scientific) under ultra-high vacuum (8.0×10^{-10} Pa). Measurements employed the monochromatic Al K_α radiation ($h\nu = 1486.8$ eV) at 12.5 kV and 16 mA emission current, with spectra acquired at 30 eV pass energy and 0.1 eV step size. Charge compensation was applied using adventitious carbon (C 1s = 284.80 eV), and all spectra represent 10-cycle signal averages to enhance signal-to-noise ratios.

FTIR Measurements.

Fourier-transform infrared (FTIR) spectroscopy was conducted using a Bruker Vertex 70 spectrometer. Sample preparation involved homogenizing the material with IR-grade potassium bromide (KBr) followed by hydraulic pressing into translucent pellets for spectral acquisition.

ICP-OES Measurements.

Inductively coupled plasma-optical emission spectrometry (ICP-OES) was performed using a plasma power of 1.2 kW, with yttrium (Y) quantified at the emission wavelength of 371.030 nm. Calibration employed Y standard solutions (0.1–10 ppm, $R^2 \geq 0.999$).

ssNMR Measurements.

^{89}Y ssNMR measurements were performed on a Bruker Avance III HD spectrometer operating at a static magnetic field strength of 14.1 T (Larmor frequency: 29.41 MHz for ^{89}Y) equipped with a 4 mm low-γ H-X double-resonance Bruker probe. The ^{1}H → ^{89}Y cross-polarization (CP) ssNMR experiments were systematically optimized using the model compound $Y(OH)_3$, which simultaneously served as the chemical shift reference ($\delta_{iso}(^{89}Y) = 68$ ppm). Experimental parameters included magic-angle spinning (MAS) rate of 5 kHz, a CP contact time of 8 ms, and a 5 s relaxation delay between successive scans. Data acquisition comprised 2048 transients to ensure adequate signal-to-noise ratio.

^{35}Cl quadrupolar Carr-Purcell-Meiboom-Gill (QCPMG) ssNMR experiments were conducted using a ^{1}H decoupling radiofrequency (RF) field strength of 38 kHz, calibrated via 1 M aqueous KCl solution (0 ppm chemical shift reference). The 90 ° pulse width (P1) was set to 6.5 μs under a power level (PLW1) of 300 W, with an interpulse delay of 20 μs within the QCPMG pulse sequence. The spike separation is 2.5 kHz. Data acquisition involved 2048 transients (ns) to enhance the sensitivity for quadrupolar ^{35}Cl nucleus.

^{79}Br quadrupolar Carr-Purcell-Meiboom-Gill (QCPMG) ssNMR experiments were conducted using a ^{1}H decoupling radiofrequency (RF) field strength of 38 kHz, calibrated via 1 M aqueous KBr (0 ppm chemical shift reference). The 90 ° pulse width (P1) was set to 4.8 μs under a power level (PLW1) of 170 W, with an interpulse delay of 20 μs within the QCPMG pulse sequence. Data acquisition involved 2048 transients (ns) to enhance sensitivity for the quadrupolar ^{79}Br nucleus.

Section S2. Additional Data and Analyses

Table S1. Comparative analysis of the adsorption performance of different adsorbents

Type	Sorbent	*N: Q_e* (mg/g)	Adsorbent (g/L)	pH	Time (min)	N: IFC (mg/L)	Temp (°C)
Functionalized carbons	UrGlu-4.520.6–2nd[5]	16.52	2	3	1200	600	25
	RHB-Mg[6]	~24	1	7	2800	400	22
	HDTMAB-RHA[7]	~22	0.1	7	240	50	25
LDHs	NiFe-MLDH/OQAS[8]	13.79	0.5	6	60	50	15
	MgZnCoAl-C[9] (calcined MgZnCoAl-LDH)	~45	0.1	6	600	400	15
	Cl–LDHs–C500[10] (calcined Cl-LDH)	15.83	0.4	5	300	67.74	25
MOFs	ASB-3[11]	~1.3	0.1	6.5	60	30	25
	LTA MOFs[12]	49.73	0.1	7	60	140	25
	FTA MOFs[13]	~55	0.1	7	60	140	25
LYH-X (this article)	LYH-Cl	44.56	2.5	7	1200	400	25
	LYH-Br	22.87	2.5	7	1200	400	25

Q_e = Nitrate equilibrium adsorption amount; IFC = Initial concentration; Temp = Ambient temperature.

Section S2. Additional Data and Analyses

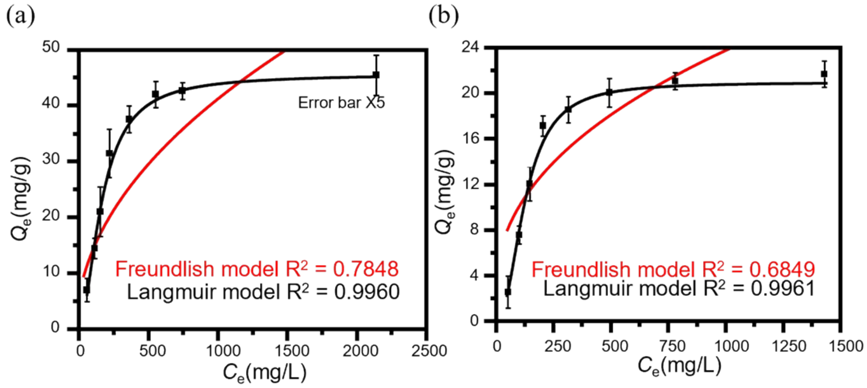

Figure S1. The adsorption isotherms of LYH-Cl (a) and LYH-Br (b) fitted with Langmuir and Freundlich equations (2.5 g/L adsorbent, C_e = 50–2100 mg/L, 12 h, 25 °C; Error bars are enlarged by a factor of five for clarity).

Section S2. Additional Data and Analyses

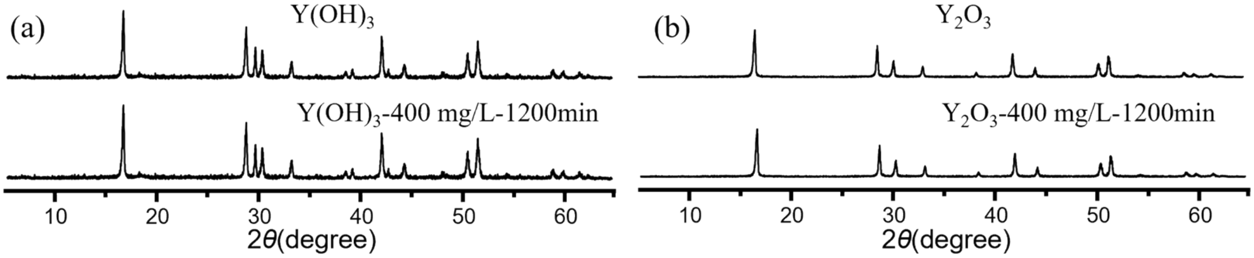

Figure S2. PXRD patterns of $Y(OH)_3$ (a) and Y_2O_3 (b) before and after nitrate adsorption (C_e = 400 mg/L, adsorption time = 1200 min, pH 7, adsorbent dose = 2.5 g/L).

Section S2. Additional Data and Analyses

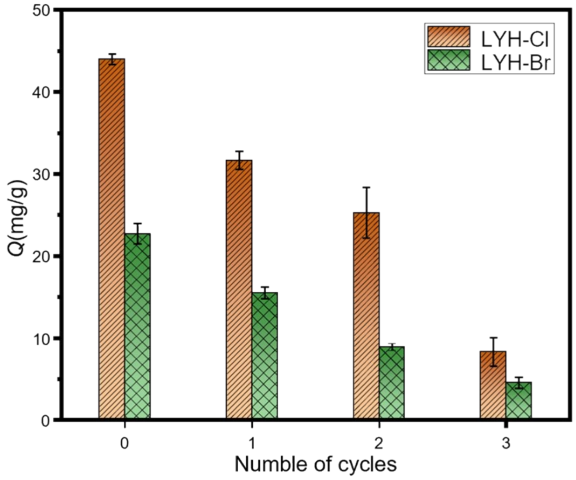

Figure S3. Cyclic adsorption-desorption performance of synthesized LYH-Cl (red) and LYH-Br (green) on NO_3^- adsorption.

Section S2. Additional Data and Analyses

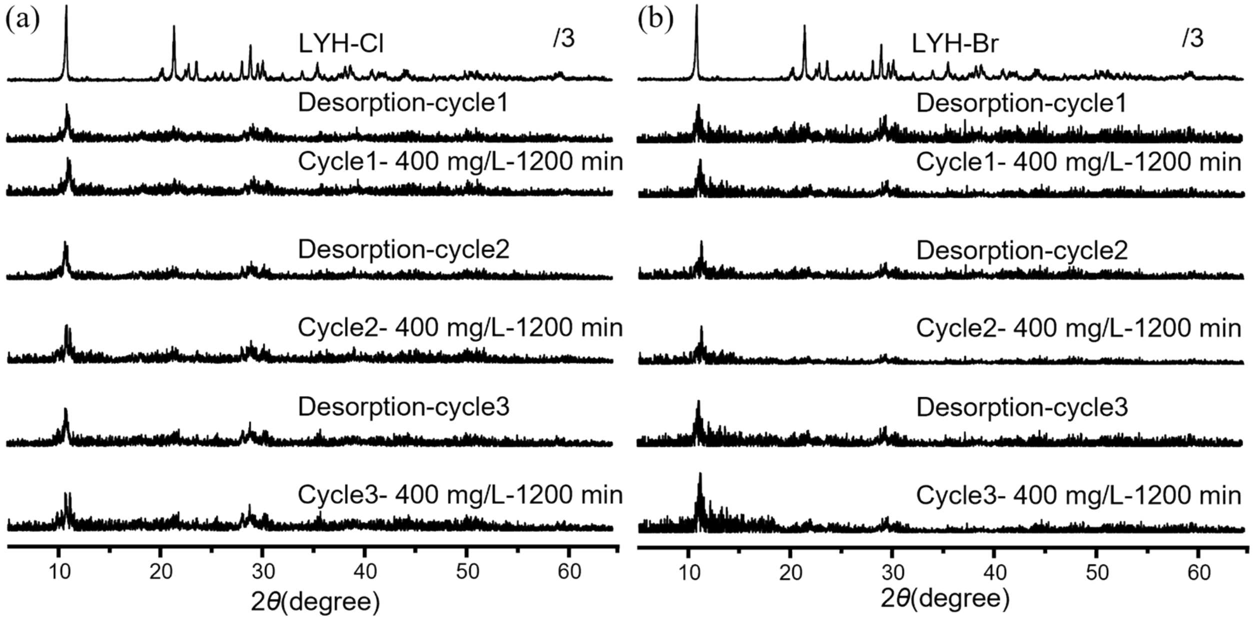

Figure S4. PXRD patterns of LYH-Cl and its desorption-cycled and re-adsorbed samples (a), and LYH-Br and its desorption-cycled and re-adsorbed samples (b). (C_e =400 mg/L, adsorption time = 1200 min, pH 7, adsorbent dose = 2.5 g/L; PXRD pattern of LYH-Cl is reduced by a factor of three with noise levels maintained for clarity of comparison).

Section S2. Additional Data and Analyses

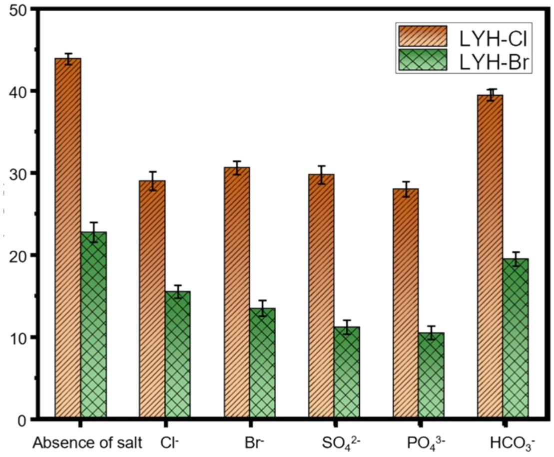

Figure S5. Impact of competitive anions on nitrate adsorption by synthesized LYH-Cl (red) and LYH-Br (green).

Section S2. Additional Data and Analyses

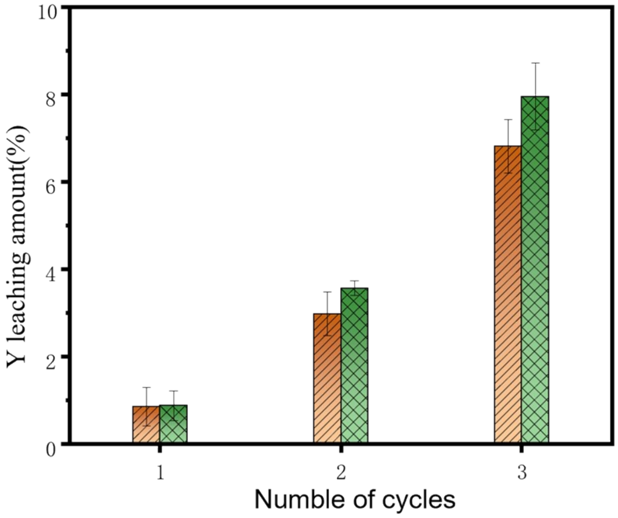

Figure S6. Y leaching amounts of LYH-Cl (red) and LYH-Br (green) after desorption in cyclic adsorption-desorption experiments.

Section S2. Additional Data and Analyses

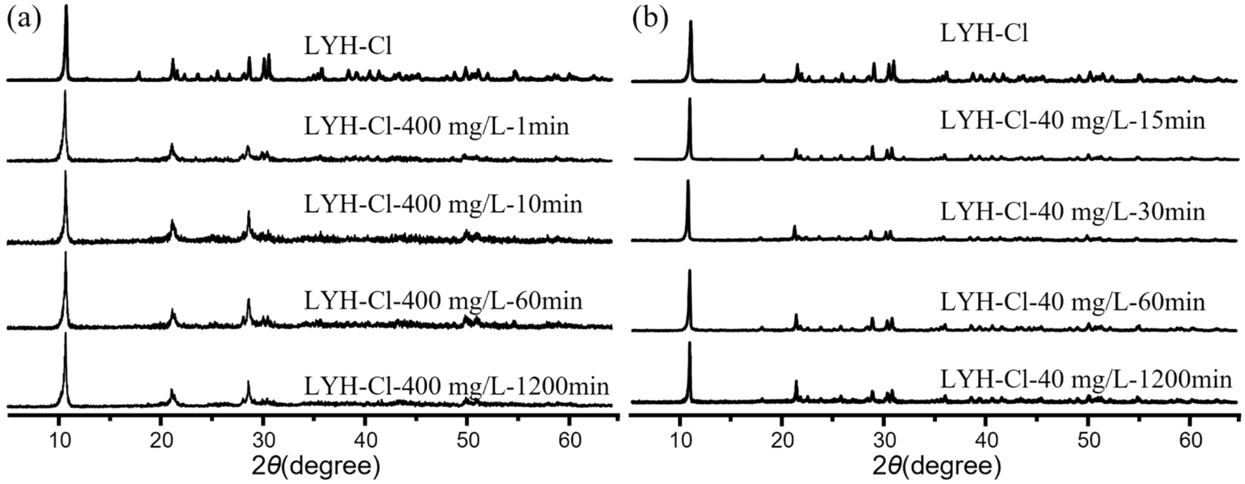

Figure S7. PXRD patterns of LYH-Cl before and after 400 mg/L-nitrate (a) and 40 mg/L-nitrate (b) adsorption (adsorption time = 1–1200 min, pH 7, adsorbent dose = 2.5 g/L).

Section S2. Additional Data and Analyses

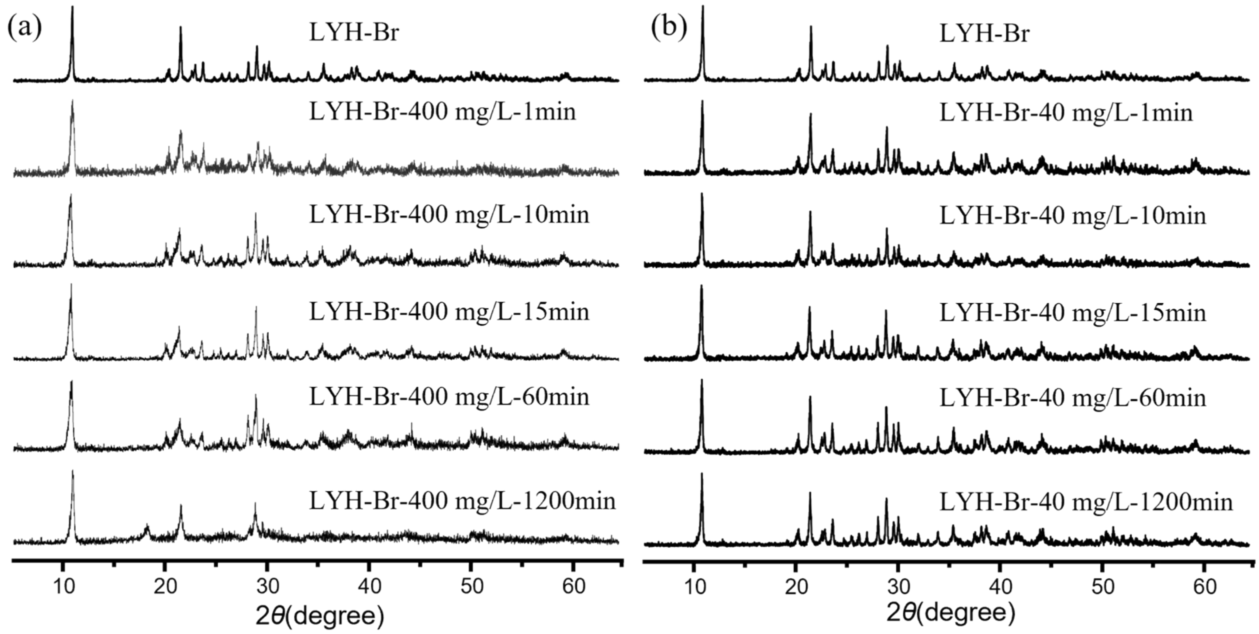

Figure S8. PXRD patterns of LYH-Br before and after 400 mg/L-nitrate (a) and 40 mg/L-nitrate (b) adsorption (adsorption time = 1–1200 min, pH 7, adsorbent dose = 2.5 g/L).

Section S2. Additional Data and Analyses

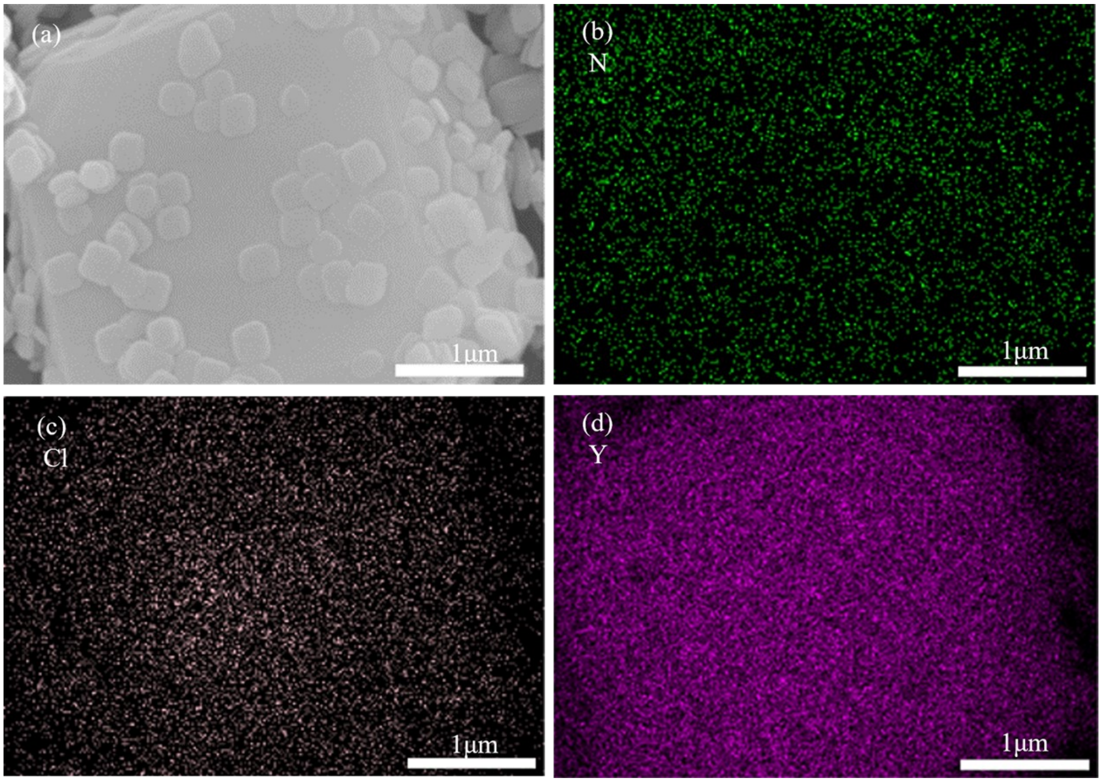

Figure S9. SEM and corresponding EDS mapping images of Y, N, and Cl. (N/Cl atomic ratio: 12.9, C_e =400 mg/L, adsorption time = 1200 min, pH 7, adsorbent dose = 2.5 g/L).

Section S2. Additional Data and Analyses

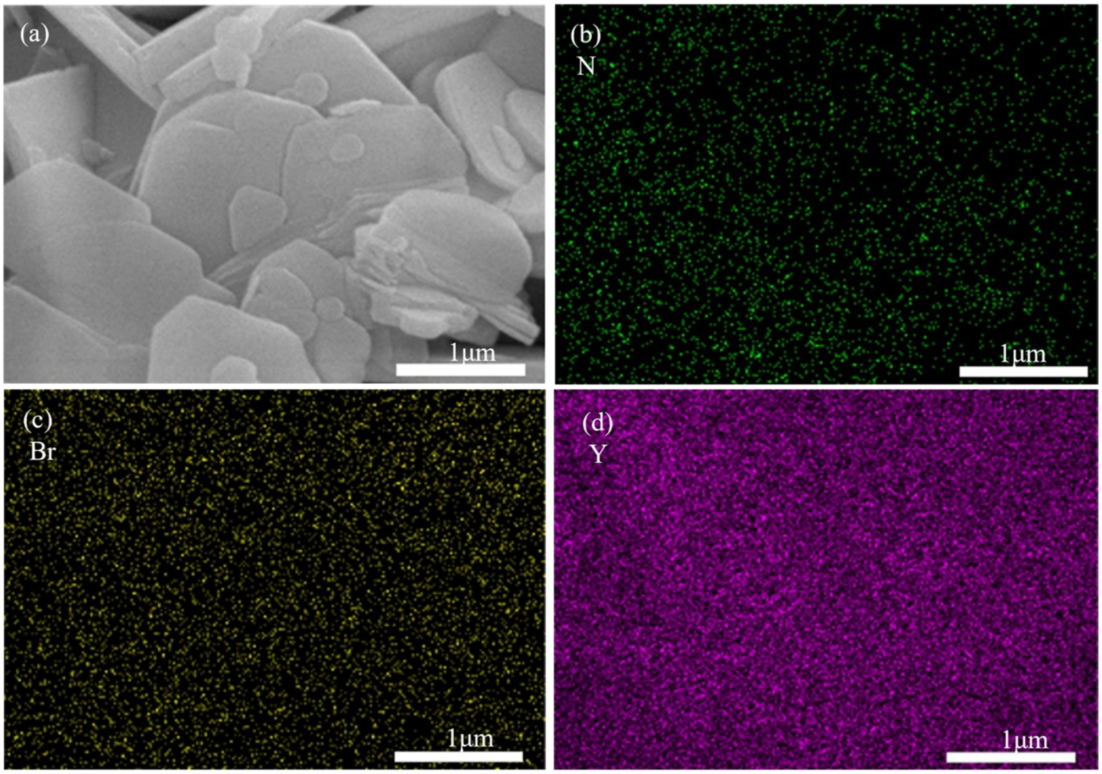

Figure S10. SEM and corresponding EDS mapping images of Y, N, and Br. (N/Br atomic ratio: 4.5, C_e =400 mg/L, adsorption time = 1200 min, pH 7, adsorbent dose = 2.5 g/L).

Section S2. Additional Data and Analyses

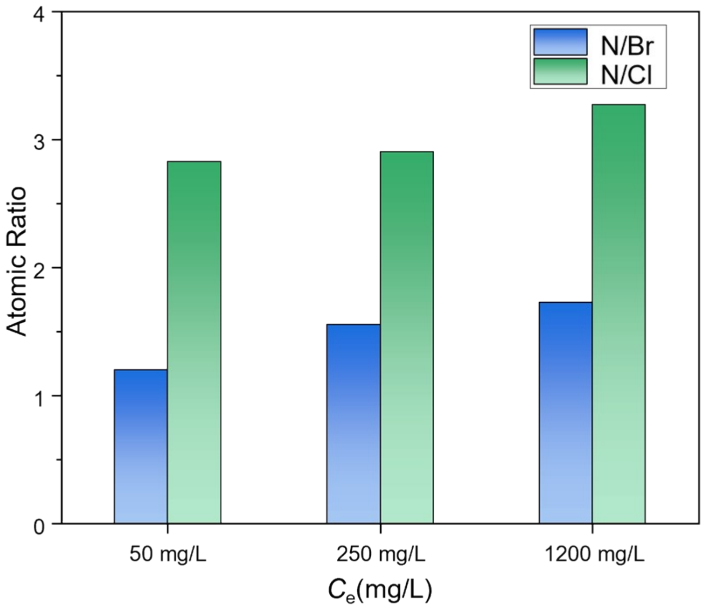

Figure S11. Comparison between the anion-exchange efficacy of LYH-Cl and LYH-Br revealed through N/Cl (green bars) and N/Br (blue bars) atomic ratios from SEM-EDS mapping, after nitrate adsorption across 50, 150, and 1200 mg/L initial concentrations. (adsorption time = 1200 min; pH 7; adsorbent dose = 2.5 g/L).

Section S2. Additional Data and Analyses

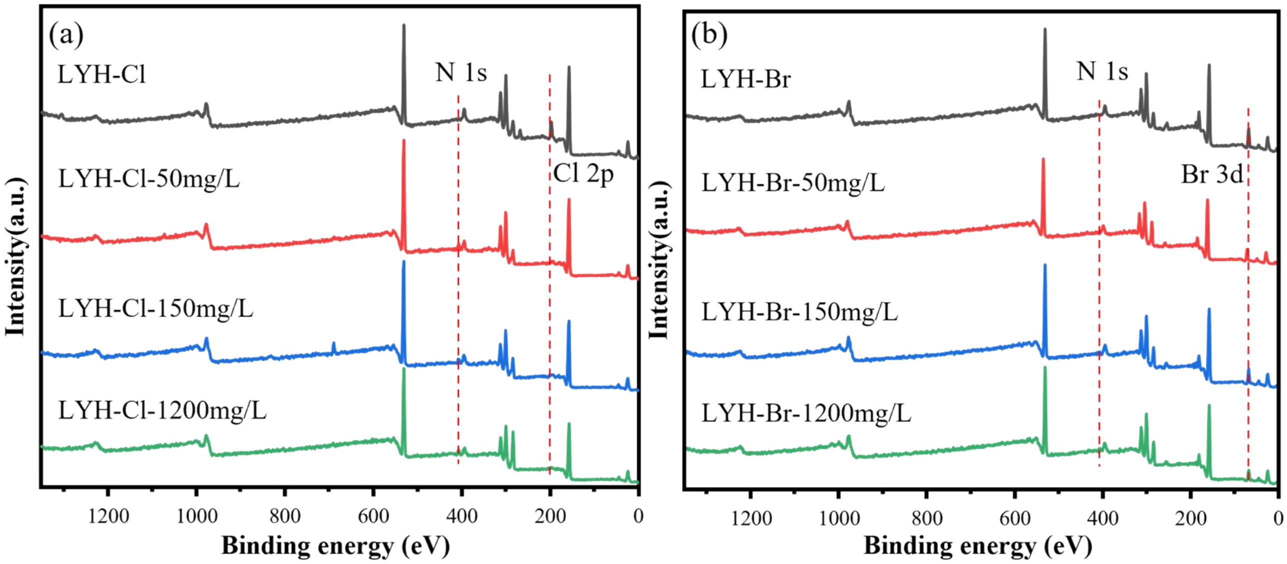

Figure S12. Full XPS spectra of LYH-Cl (a) and LYH-Br (b) before and after nitrate adsorption. (C_e = 50-1200 mg/L, 12 h, pH 7, adsorbent dose = 2.5 g/L).

Section S2. Additional Data and Analyses

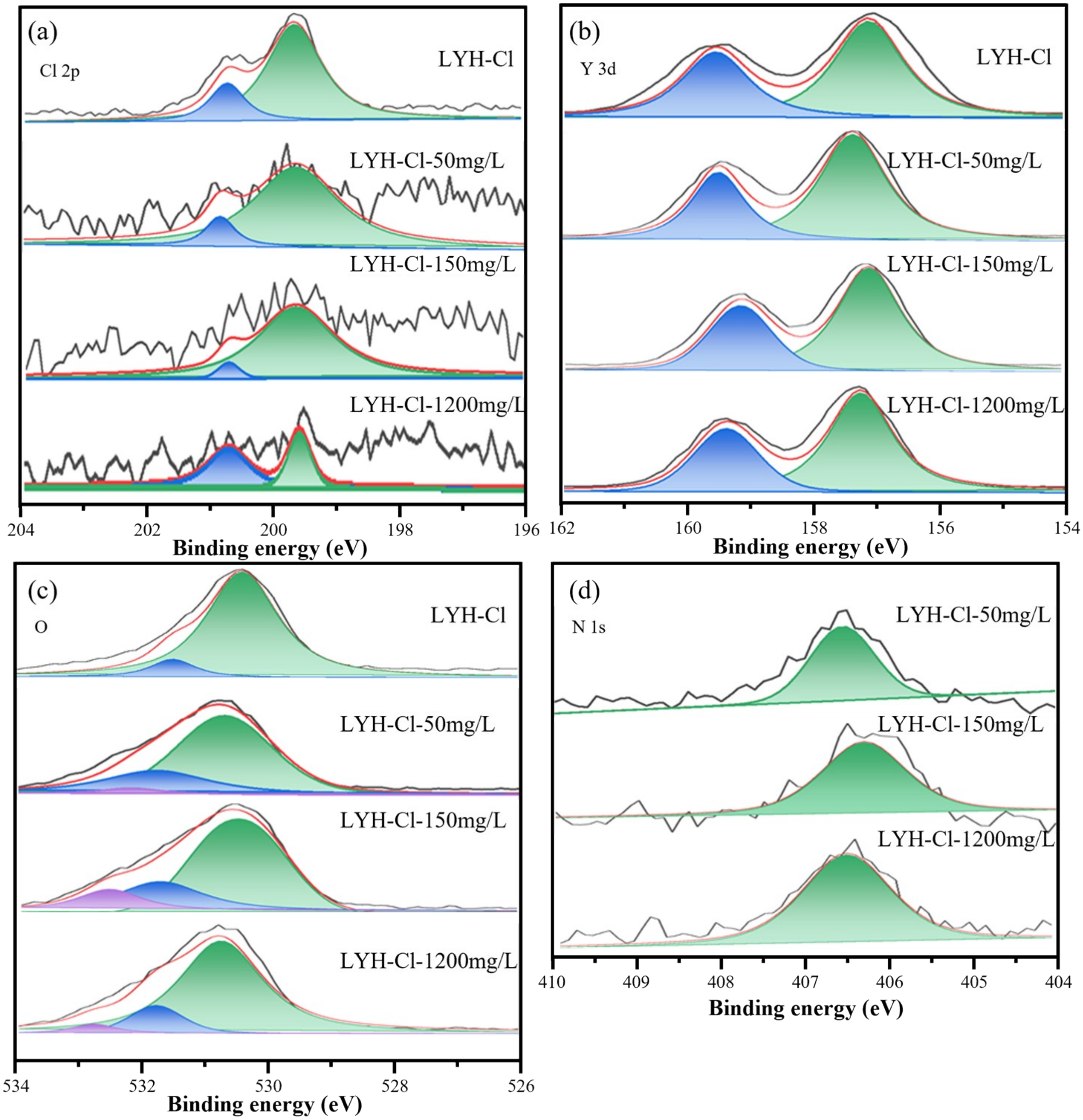

Figure S13. Experimental and fitted XPS spectra of LYH-Cl before and after nitrate adsorption for (a) Cl 2p, (b) Y 3d, (c) O 1s, and (d) N 1s core levels. (C_e = 50/150/1200 mg/L, adsorption time = 1200 min; pH 7; adsorbent dose = 2.5 g/L).

Section S2. Additional Data and Analyses

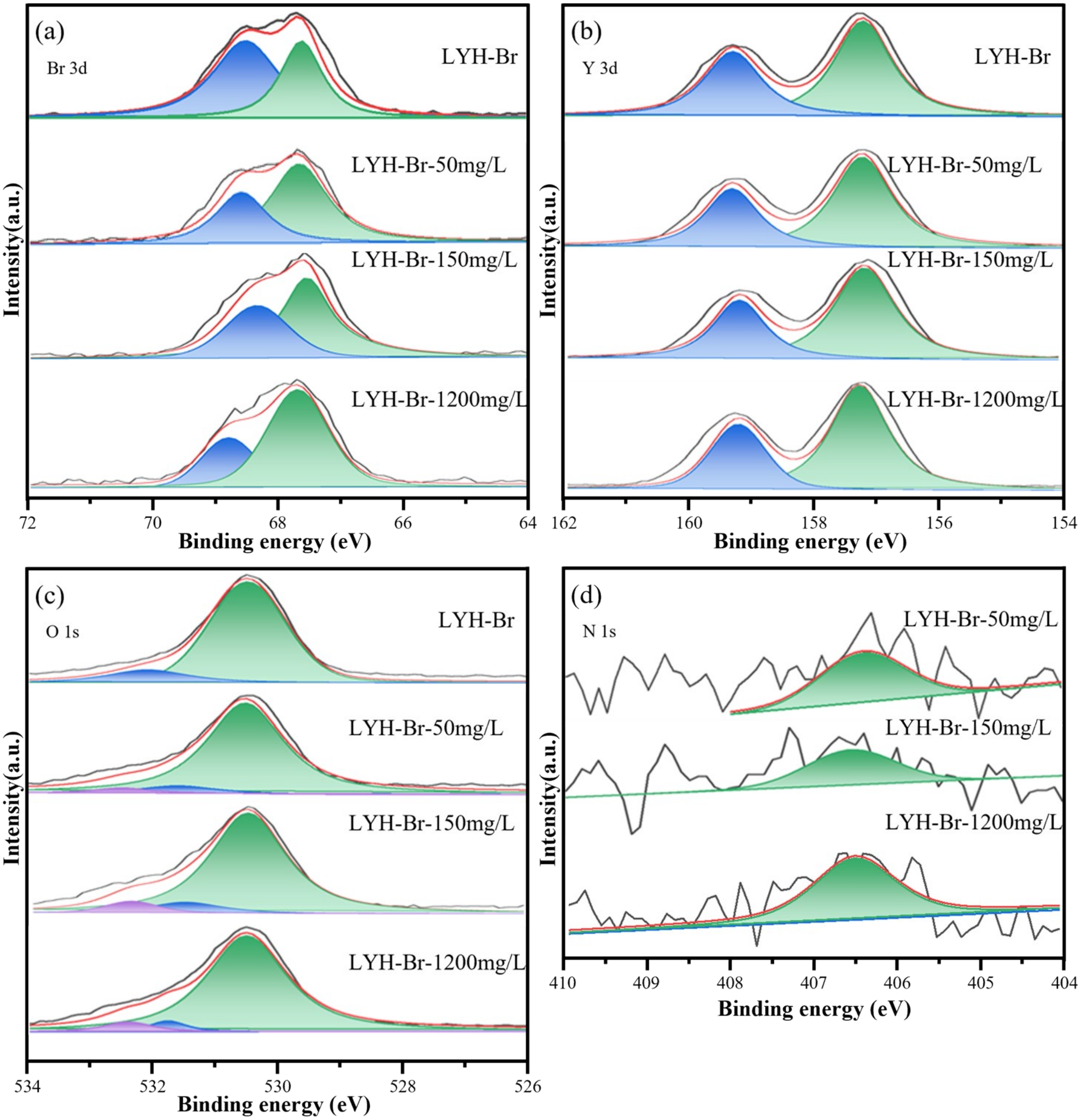

Figure 14. Experimental and fitted XPS spectra of LYH-Br before and after nitrate adsorption for (a) Cl 2p, (b) Y 3d, (c) O 1s, and (d) N 1s core levels. (C_e = 50/150/1200 mg/L, adsorption time = 1200 min; pH 7; adsorbent dose = 2.5 g/L).

Section S2. Additional Data and Analyses

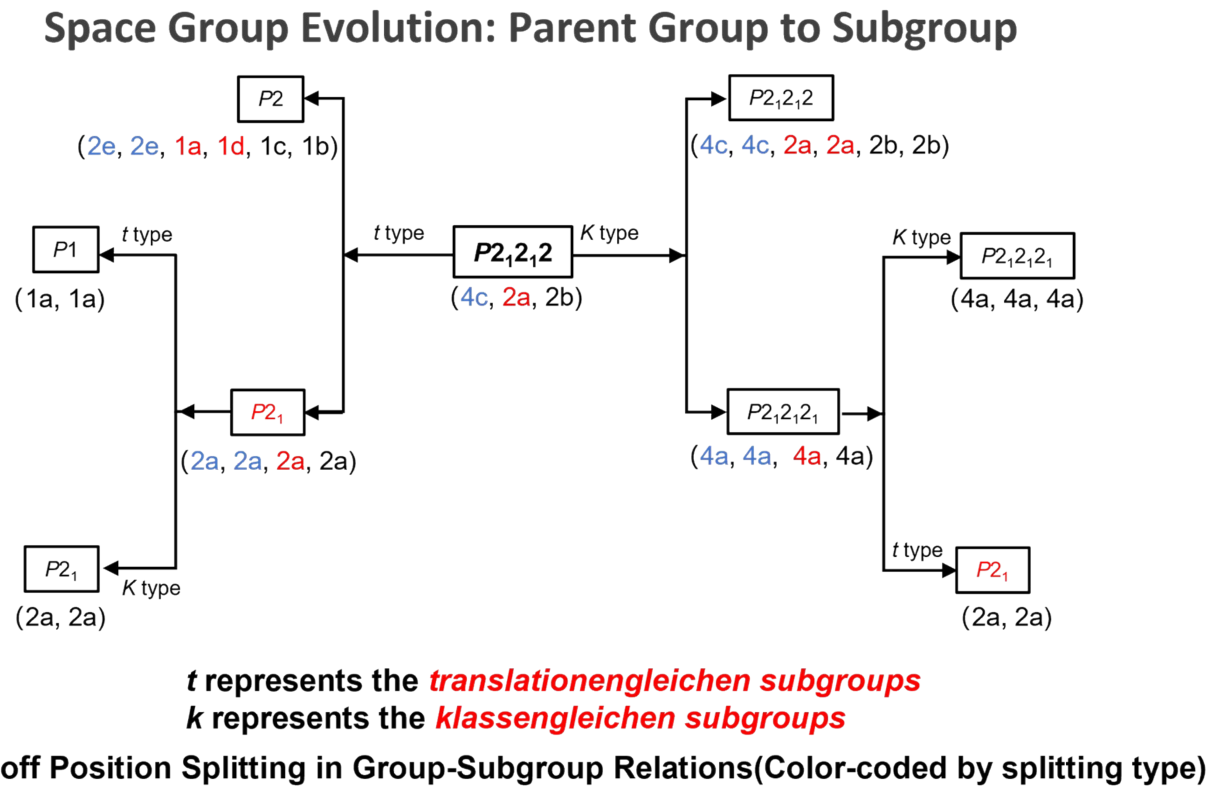

Scheme S1. Symmetry evolution pathway of orthorhombic $P2_12_12$ space group.

References

(1) Feng, Z.; Xiao, D.; Liu, Z.; Hou, G.; Xu, J. "X Factor" in the Structure and Anion Exchange of Layered Yttrium Hydroxides. *J. Phys. Chem. C* **2021**, *125* (13), 7251-7258.

(2) Wu, K.; Xu, J. The Ordering and Arrangement of Intercalated Carboxylate Ions in Anion-Exchangeable Layered Yttrium Hydroxides. *Eur. J. Inorg. Chem.* **2024**, *27* (35), e202400477.

(3) Liu, Y.; Sheng, X.; Ding, H.; Xu, J. A comprehensive solid-state NMR and theoretical modeling study to reveal the structural evolution of layered yttrium hydroxide upon calcination. *J. Magn Reson Open* **2024**, *20*, 100155.

(4) Zahid, M.; Zhang, D.; Xu, X.; Pan, M.; ul haq, M. H.; Reda, A. T.; Xu, W. Barbituric and thiobarbituric acid-based UiO-66-NH2 adsorbents for iodine gas capture: Characterization, efficiency and mechanisms. *J. Hazard. Mater.* **2021**, *416*, 125835.

(5) Wang, J.; Amano, Y.; Machida, M. Enhancement of nitrate adsorption from aqueous solutions by glucose-derived nitrogen-doped carbonaceous adsorbent. *J. Anal. Appl. Pyrolysis* **2025**, *189*, 107100.

(6) Lugo-Arias, J.; González-Álvarez, J.; Maturana, A.; Villa-Parejo, J.; Barraza-Heras, C. Removal of nitrate and phosphate from aqueous solutions using bioadsorbents derived from agro-industrial wastes of rice husk and corn stalk. Biomass Convers. Biorefin. **2025**, doi: 10.1007/s13399-025-06720-4.

(7) Bahrami, M.; Amiri, M. J. Nitrate removal from contaminated waters using modified rice husk ash by Hexadecyltrimethylammonium bromide surfactant. *React. Kinet., Mech. Catal.* **2022**, *135* (1), 459-478.

(8) Lu, S.; Zhu, Q.; Li, R. Selective adsorption of nitrate in water by organosilicon quaternary ammonium salt modified derived nickel-iron layered double hydroxide: Adsorption characteristics and mechanism. *J. Colloid Interface Sci.* **2023**, *652*, 1481-1493.

(9) Elhachemi, M.; Chemat-Djenni, Z.; Chebli, D.; Bouguettoucha, A.; Amrane, A. Synthesis and physicochemical characterization of new calcined layered double hydroxide Mg Zn Co Al-CO_3; classical modeling and statistical physics of nitrate adsorption. *Inorg. Chem. Commun.* **2022**, *145*, 109549.

(10) Mariska, S.; Jin-Wei, Z.; Chien, H. H.; Ngoc, D. M.; Hai, N. D.; Chao, H.-P. Adsorptive removal of phosphate and nitrate by layered double hydroxides through the memory effect and in situ synthesis. *Appl. Water Sci.* **2025**, *15* (2), 42.

(11) Li, S.; Ma, X.; Ma, Z.; Dong, X.; Wei, Z.; Liu, X.; Zhu, L. Mg/Al-layered double hydroxide modified biochar for simultaneous removal phosphate and nitrate from aqueous solution. *Environ. Technol. Innovation* **2021**, *23*, 101771.

(12) Aswin Kumar, I.; Jeyaseelan, A.; Viswanathan, N.; Naushad, M.; Valente, A. J. M. Fabrication of lanthanum linked trimesic acid as porous metal organic frameworks for effective nitrate and phosphate adsorption. *J. Solid State Chem.* **2021**, *302*, 122446.

(13) Kumar, I. A.; Jeyaseelan, A.; Ansar, S.; Viswanathan, N. A facile synthesis of 2D iron bridged trimesic acid based MOFs for superior nitrate and phosphate retention. *J. Environ. Chem. Eng.* **2022**, *10* (2), 107233.